Mapping brain metabolism, connectivity and neurotransmitters topography in early and late onset dementia with Lewy bodies

Silvia Paola Caminiti
IRCCS Ospedale San Raffaele
Alice Galli
Vita-Salute San Raffaele University
Lorenzo Jonghi-Lavarini
University of Milano-Bicocca
Cecilia Boccalini
Vita-Salute San Raffaele University
Nicolas Nicastro
University Hospital of Geneva
Valentina Garibotto
University Hospital of Geneva
Daniela Perani
perani.daniela@hsr.it

Vita-Salute San Raffaele University

Research Article

Keywords: Lewy Body Disease, disease onset, brain metabolism, connectivity, serotonin

Posted Date: June 26th, 2023

DOI: https://doi.org/10.21203/rs.3.rs-3083821/v1

Additional Declarations: No competing interests reported.

Version of Record: A version of this preprint was published at Parkinsonism & Related Disorders on May 1st, 2024. See the published version at https://doi.org/10.1016/j.parkreldis.2024.106061.

Abstract

Background:

Early- and late-onset dementia with Lewy bodies (EO-DLB and LO-DLB) are similar in terms of core symptoms. However, LO-DLB presents with more amnestic deficits, while EO-DLB shows a rapid cognitive decline and more severe neuropsychiatric symptoms at onset. A contribution of neurotransmitter dysfunction was suggested but never explored, as a possible factor contributing to the reported clinical differences. By using FDG-PET brain metabolism imaging, we aimed to assess the differences between EO-DLB and LO-DLB regarding brain hypometabolism, related neurotransmitter functional topography, and metabolic connectivity.

Methods:

We included a total of 62 patients, 21 EO-DLB and 41 LO-DLB patients. Statistical parametric mapping (SPM) voxel-wise comparison with a validated dataset of healthy controls (N=112) provided brain hypometabolism patterns. A metabolic connectivity analysis assessed whole-brain and resting-state network (RSN) alterations. Furthermore, we used the JuSpace toolbox to evaluate the correlations between neurotransmitter pathways topography and brain hypometabolism.

Results:

Both EO- and LO-DLB groups showed typical bilateral occipito-parieto-frontal hypometabolism. Direct between-group comparison revealed a more severe hypometabolism in posterior cingulate cortex (PCC), precuneus, and occipital cortex for EO-DLB and a more severe hypometabolism in fronto-insular cortices for LO-DLB. Metabolic connectivity analysis showed significant reductions in posterior brain regions in both clinical groups compared to controls, as well as connectivity increases in the EO-DLB only. There were differences in the involvement of temporo-parietal and occipital pathological nodes. Specific RSN vulnerabilities were observed in the executive, default mode and limbic networks for EO-DLB and in the attentional network for LO-DLB.

The spatial association analysis based on the metabolic differences in neurotransmission showed significant correlations with acetylcholine, gamma-aminobutyric acid (GABA), serotonin, dopamine maps, and hypometabolism in both EO and LO-DLB groups. Of note, the between-group comparison showed a higher correlation for the EO-DLB in the presynaptic serotonergic system. Overall, this indicates the biochemical involvement of metabolic impairment.

Conclusions:

This metabolic imaging study indicates similarities and differences between EO- and LO-DLB, both in terms of brain hypometabolism, across different neurotransmission networks, and altered connectivity, adding novel biological evidence to the DLB syndromes.

Background

Up to 30% of people diagnosed with dementia develop clinical symptoms at a younger age [1]. Early onset (EO) dementia refers to a condition starting before the age of 65, often characterized by more marked behavioral and psychiatric symptoms, and a higher mortality than late-onset (LO) dementia [2]. EO and LO dementia with Lewy bodies (DLB) are similar in terms of core clinical symptoms (i.e., visual hallucinations, parkinsonism, fluctuating cognition, and REM sleep behavior disorder (RBD) [3, 4], however, LO-DLB present more severe memory deficits than EO-DLB, while EO-DLB has a quicker decline and neuropsychiatric features at the beginning [5]. The EO-DLB has been poorly investigated yet, however, some specific prodromal clinical features are reported, namely a history of depression that can predate an early onset of DLB [6]. Recently, a differential contribution of neurotransmitter changes was suggested as a possible explanation for the reported clinical features in DLB. For example, some authors proposed a serotonergic neurotransmission deficit as the main monoaminergic etiology of depression in DLB [7, 8]. To date, the possible molecular imaging differences between EO-DLB and LO-DLB have not been explored.

FDG-PET brain hypometabolism represents a suggestive biomarker for early and differential diagnosis of DLB[9]. Brain hypometabolism is an early biomarker of neurodegeneration, which has been associated with a variety of neuropathological events, including impaired neurotransmitter release [10, 11]. Moreover, growing evidence suggests that molecular and pathological alterations consistently impact large-scaled brain networks [12]. Thus, this study aimed to explore i) FDG-PET brain hypometabolism patterns characterizing EO-DLB and LO-DLB; ii) metabolic connectivity in large-scale resting-state networks; iii) FDG-PET brain hypometabolism patterns spatially associated with the topography of specific brain neurotransmitter systems.

Methods

Patients

We included N = 62 patients with a clinical diagnosis of probable DLB retrospectively evaluated from the clinical and imaging database of San Raffaele Hospital Milan, Italy, and Geneva University Hospitals, Switzerland. Clinical diagnosis of probable DLB was made according to the diagnostic criteria of McKeith et al. (2017), i.e., dementia in association with the presence of at least two core symptoms (cognitive fluctuations, visual hallucinations, RBD or parkinsonism) or one core symptom together with one indicative biomarker (e.g., low dopamine transporter uptake at SPECT)[3]. Participants were subsequently stratified into two clinical groups according to age at onset (EO-DLB $\leq$ 65 years, LO-DLB age at onset > 65 years)[13]. In addition, we collected the prevalence of neuropsychiatric symptoms (i.e., depression, apathy, irritability, and anxiety) considering neuropsychiatric index (NPI) scores or medical records. Cerebrospinal Fluid (CSF) examination of β-amyloid (1–42), total-Tau, and phospho-Tau, were available for 52% (33/62). Between-group differences in demographical and clinical measures were assessed by applying ANOVA and Chi-square test for continuous and discrete variables, respectively.

FDG-PET procedure

All participants underwent FDG-PET scan, according to the European Association of Nuclear Medicine guidelines (ref). Images performed at the Nuclear Medicine Unit, San Raffaele Hospital (Milan), were acquired using the same Discovery STE PET (3.27-mm thickness; in-plane full-width at half maximum (FWHM) 5.55-mm) manufactured by GE Healthcare. FDG-PET images from the nuclear medicine and molecular imaging division at Geneva University Hospitals were acquired with Biograph128 mCT, Biograph128 Vision 600 Edge, or Biograph64 TruePoint PET scanners (Siemens Medical Solutions, USA). All scanners were harmonized regarding their performance and reconstructions and cross-calibrated.

Static emission images were acquired 30 to 45 min after injecting 185–250 MBq of [18F]FDG via a venous cannula. This post-injection time interval allows obtaining an equal distribution of the tracer across the entire brain, with negligible blood flow-dependent differences, thus achieving an optimal signal-to-noise ratio. The duration of scan acquisition was 15–20 min.

Pre-processing

A rigorous quality control process was performed to check potential artifacts (e.g., acquisition issues, excessive patient motion) and issues related to technical characteristics, such as the use of comparable reconstruction algorithms. Then, FDG-PET images of patients and controls were normalized to the optimized FDG-PET template[14], using Statistical Parametric Mapping 12 (SPM12) (https://www.fil.ion.ucl.ac.uk/spm/). They were then scaled to the global mean of the activity within the brain and finally smoothed with an isotropic 3D Gaussian kernel (8 mm FWHM), according to the validated pipeline proposed for our single-subject SPM-based analysis [15].

Brain Hypometabolism Maps

The procedure consists of a two-sample t-test comparison of a single patient's image to a large database of 112 healthy controls (HC) using age as a nuisance covariate ($p < 0.05$, minimum cluster extent $k = 100$ voxels). See[16] for a detailed description of the procedure.

Each subject's SPM-t hypometabolism maps were then converted into the normal z-like distribution (SPM-z maps) with MATLAB R2021b (Mathworks Inc., Sherborn, MA, USA). Low z-scores (< 0) indicated more severe regional hypometabolism compared to HC. By considering SPM z-maps, regional hypometabolism values (SPM z-scores) were extracted from a set of predefined (DLB typical hallmarks [17]) and data-driven (based on the results of univariate SPM group analysis) regions of interest (ROIs), namely Inferior, Middle and Superior Occipital Lobe, Calcarine Cortex, Lingual Gyrus, Fusiform Gyrus, Superior and Inferior Temporal Gyrus, Inferior and Superior Parietal Lobules, Middle Frontal Gyrus, Posterior Cingulate Cortex (PCC), Insula, Supplementary Motor Area and Parahippocampus. We also calculated the Cingulate Island Sign (CIS) ratio that was derived by dividing the FDG uptake in the PCC with that in the precuneus and cuneus[18]. The ROIs were derived from the Automated Anatomical Labelling (AAL) Atlas[19]. Between-group differences in brain hypometabolism within the DLB ROIs were assessed by means of a two-sample t-test on Statistical Package for Social Sciences (SPSS).

To describe group-level brain hypometabolism pattern characterizing the whole DLB cohort, patients' normalized images were compared to a set of 112 HC (age = 64.7 ± 9.3; Sex (male/female) = 53/59). The HC dataset was previously developed and validated by our group for the extraction of hypometabolism maps in individual neurological patients or groups [16]. Group comparison was performed by means of a two-sample t-test on SPM12 setting the statistical threshold at p = 0.05, family-wise error (FWE)-corrected for multiple comparisons. Only clusters containing more than 100 voxels were deemed to be significant. The same statistical design was applied to compare each DLB group with HC, as well as a head-to-head comparison of EO-DLB and LO-DLB. All SPM group analyses were performed considering age as a nuisance variable.

Metabolic Connectivity analysis

Metabolic connectivity analysis was applied to investigate the architecture of the whole-brain network and resting state networks for both DLB groups, and for the HC group for comparison. A group of 50 HC (for proper numerosity given the analysis) was randomly selected for comparison (mean age 65 yrs ± 8).

Whole-brain network - The whole-brain network was constructed considering the 116 cortical, subcortical, and cerebellar ROIs of the AAL atlas (network nodes) [19]. FDG uptake normalized by global brain uptake was extracted from each node to create a subject-by-nodes matrix for each group. Then, an adjacency matrix was obtained for each group by applying a linear correlation between nodes across subjects ($p < 0.001$). Between-group comparison (EO-DLB vs. HC; LO-DLB vs. HC) was performed by applying a z-test to Fisher's transformed correlation coefficients ($p < 0.001$). For each obtained node, we computed the mean absolute value of the z-scores resulting in significantly altered in the DLB groups in comparison to HC.

The analysis was run using MATLAB software (http://it.mathworks.com/products/matlab/) Mathworks Inc., Sherborn, Mass., USA).

Resting state network - Voxel-wise seed-based interregional correlation analysis (IRCA) was applied to derive metabolic connectivity in specific resting state networks (RSNs). This method was previously validated for FDG-PET data[20] and allows to derive RSNs starting from proper seed regions. In this study, we selected seed regions for large-scale networks as previously identified by extensive literature: the ventro-medial frontal cortex for the anterior default mode network (aDMN); the PCC and precuneus for the posterior DMN (pDMN)[21]; the dorsolateral prefrontal cortex (dlPFC) for the executive network (EXN)[22]; the angular and supramarginal gyri for the attentional network (ATN)[23], and the amygdala for the limbic network (LIN)[23]. Seed regions of interest were derived from the AAL atlas and functional RSNs atlas[23], using the REX toolbox to extract the mean regional metabolism value from each seed. For each network, the seed uptake was set as the variable of interest in a multiple regression model in SPM12, entering age as covariate of nuisance- to test whole-brain voxel-wise correlations, setting the p-value at < 0.001, with kep value > 100 voxels.

Metabolic Spatial Distribution of Neurotransmitter Systems

We used JuSpace toolbox[24] for our dataset to test whether brain hypometabolism was spatially correlated with the distribution of specific neurotransmitter systems. We selected each subject's hypometabolism z-map (EO-DLB vs. HC; LO-DLB vs. HC) to compute Spearman correlations with provided PET and SPECT intensity maps of neurotransmitter systems. In detail, PET/SPECT intensity maps covered the following receptor types: 5-HT1a (serotonin 5-hydroxytryptamine receptor subtype 1a), 5-HT1b (5-HT subtype 1b), 5-HT4 (5-HT subtype 4), dopamine transporter (DAT), GABAa (gamma-aminobutyric acid), NAT (noradrenaline transporter) SERT (serotonin transporter), and AChT (acetylcholine transporter). These maps were derived from data obtained with specific radiotracers [27]. Specifically, the SERT map was obtained from HC images of ^{11}C-DASB PET, a selective in vivo marker of 5-hydroxytryptamine transporter (5HTT) binding in humans [45].The neuromorphometric atlas from SPM12 was used to extract mean metabolic regional values from the input images to be correlated with the regional values of neurotransmitter maps. Then, we computed option 8 (extracts mean value per atlas region for each file from list 1 and compares correlation coefficients for all images against null distribution) to compare the obtained Fisher's z-scores correlation coefficients against null distribution using a one-sample t-test. Exact permutation-based p-values (with N = 10.000 permutations) were requested for this analysis.

The obtained Fisher's z-scores were then entered into a two-sample t-test on SPSS to directly compare the two DLB groups. Moreover, in a posthoc analysis, the Fisher's z-scores of the neurotransmitter system which significantly differentiated the two groups (see Results) were entered together with the individual SPM z-maps into a linear regression model to identify the brain hypometabolic regions driving the between-group neurotransmitter differences. We set statistical threshold at $p < 0.05$, FWE-corrected for multiple comparisons, and we considered only clusters containing more than 100 voxels to be significant.

Data Availability

The data that support the findings of this study are available from the corresponding authors upon reasonable request.

Results

The two DLB groups were similar regarding clinical and demographical features, except age at onset ($p<0.001$), by definition (see **Table 1**). DLB groups were comparable for frequency of neuropsychiatric symptoms, namely depression ($p=0.25$), apathy ($p=0.29$), irritability ($p=0.99$), and anxiety ($p=0.92$). CSF p-tau load resulted higher in the LO-DLB than EO-DLB group ($p=0.03$). REM sleep behavior disorder was more frequent in the LO-DLB group (49% vs 21%, $p=0.07$).

Table 1- Clinical, CSF and demographical features in the two studied groups at the time of PET exam.

	EO-DLB	LO-DLB	p-value
N	21	41	
Age (years)	59.1 ± 3.8	74.8 ± 5.9	**<0.001**
Sex (female/male)	8/13	13/28	0.62
Disease Duration (years)	2.7± 1.7	2.3 ± 1.4	0.45
Education (years)	10.6 ± 3.3	10.7 ± 4.8	0.95
MMSE, total	19.8 ± 4.9	19.1 ± 4.8	0.65
CSF Ab 1-42 (z-score) †	-0.8±1.3	0.04±0.8	0.36
CSF total-Tau (z-score) †	-0.2±0.8	0.08±1.1	0.63
CSF total-Tau/Ab 1-42 (z-score) †	0.42±1.4	-0.08±0.9	0.44
CSF phosphorylated-Tau (z-score) †	-0.5±0.7	0.2±1.1	**0.03**
CSF phosphorylated-Tau/Ab 1-42 (z-score) †	-0.03±0.5	0.01±1.09	0.95
Neuropsychiatric Features, Number and (%)°			
Depression	7 (54%)	12 (35%)	0.25
Apathy	8 (62%)	15 (44%)	0.29
Irritability	5 (39%)	13 (38%)	0.99
Anxiety	4 (31%)	12 (32%)	0.92
Core DLB criteria, Number (%)			
Parkinsonism	13 (87%)	36 (88%)	0.91
Fluctuating Cognition	7 (50%)	20 (49%)	0.94
Visual Hallucinations	7 (50%)	26 (63%)	0.38
REM sleep behavior disorder	3 (21%)	20 (49%)	0.07

† *CSF z-scores are calculated based on the distribution of the Milan and Geneva DLB groups. ° Data available for 47 out of 62 DLB participants. MMSE= Mini-Mental State Examination; CSF= cerebrospinal fluid; DLB = dementia with Lewy Bodies. Numbers in bold indicate significant results.*

Group-analysis

SPM voxel-wise analysis showed a significant hypometabolism in middle and superior occipital lobe, angular gyrus, supramarginal gyrus, precuneus, inferior frontal gyrus and middle frontal gyrus, bilaterally (**Figure 1**). Regarding direct comparison of DLB groups, we found no differences in terms of brain hypometabolism in the DLB core regions (**Table 2**). However, differences emerged in extra-DLB typical

regions. Namely, the EO-DLB group showed a more severe hypometabolism in the superior parietal cortex and PCC. Instead, the LO-DLB group presented a significant hypometabolism in the insula, supplementary motor area, and parahippocampal gyrus when compared to the EO-DLB group (**Figure 1** and **Table 2**).

Table 2 – Comparisons of brain hypometabolism (Z scores) between EO-DLB and LO-DLB groups

	EO-DLB	LO-DLB	p-value
ROIs			
Angular Gyrus	2.25±1.36	2.02±0.9	0.49
Calcarine Cortex	0.82±0.77	0.94±0.58	0.48
Middle Frontal Gyrus	0.51±0.91	0.53±0.81	0.95
Fusiform Gyrus	-0.37±0.59	-0.16±0.65	0.23
Superior Temporal Gyrus	0.006±0.96	0.37±82	0.12
Inferior Temporal Gyrus	0.28±0.82	0.32±0.71	0.84
Lingual Gyrus	0.49±0.75	0.57±0.60	0.66
Inferior Occipital Lobe	1.44±0.68	1.29±0.89	0.52
Middle Occipital Lobe	1.66±0.88	1.45±0.82	0.35
Superior Occipital lobe	1.16±0.71	0.91±0.78	0.12
Superior Parietal Cortex	1.22±0.91	0.84±0.86	**0.04**
Posterior Cingulate Cortex	0.81±0.98	0.76±0.72	**0.03**
Insula	-1.14±0.87	-0.63±0.64	**0.01**
Supplementary Motor Area	-0.23±0.73	-0.12±0.72	**0.03**
Parahippocampal Gyrus	-1.47±0.83	-0.97±0.78	**0.01**
CIS	0.43±0.03	0.42±0.03	0.30

CIS = cingulate island sign; EO-DLB= early-onset dementia with Lewy bodies; LO-DLB= late-onset dementia with Lewy bodies. Significant p-values are reported in bold.

Metabolic connectivity analysis

Overall, comparable whole-brain connectivity alterations were found in the two clinical groups as compared to HC (**Figure 2**). We showed decreases and increase in connectivity, the latter was more evident in the posterior regions of the EO-DLB group. Some discrepancies were also evident in the pathological nodes. Namely, the EO-DLB showed pathological nodes in precuneus, inferior and superior

parietal cortex, angular gyrus, inferior temporal cortex and middle occipital cortex, the LO-DLB, in the lingual gyrus, inferior occipital cortex, fusiform, middle temporal cortex, and cerebellar vermis.

The RSN metabolic connectivity in EO-DLB, LO-DLB and HC as reference, revealed: i) for the EO-DLB, reduced connectivity in the frontal components of the EXN, aDMN and pDMN and in the LIN, a loss of connectivity in thalamus and pons and an increased connectivity between ventral putamen and amygdala; ii) for the LO-DLB, a loss of connectivity in the ATN, involving the dorsolateral prefrontal cortex (**Figure 3**).

Spatial Distribution of Neurotransmitter Systems

The hypometabolism z-score maps were spatially correlated with AChT (r=-0.368, p <0.001), GABAa (r=0.331, p=0.004), SERT (r=-0.256, p<0.001), and DAT (r=-0.220, p<0.001) neurotransmitter maps in the whole DLB group.

As for the EO-DLB group, we found a significant association between hypometabolism z-score maps and the distribution of AChT (r=-0.414, p <0.001), GABAa (r=0.348, p=0.005), SERT (r=-0.326, p<0.001), DAT (r=-0.292, p<0.001) and 5HT4 (r=-0.133, p=0.04) maps.

As for the LO-DLB group, hypometabolism z-score maps were significantly associated with the distribution of AChT (r=-0.345, p<0.001), GABAa (r=0.333, p=0.004), SERT (r=-0.22, p<0.001), and DAT (r=-184, p=0.002) maps (**Figure 4**).

The resulting negative correlation coefficients indicate that the hypometabolism characterizing each group was present in structures specific for each neurotransmitter.

The post-hoc direct comparison between EO and LO-DLB Fisher's z scores showed differences only in the SERT map (p=0.029), and the largest hypometabolism cluster driving the relationship between hypometabolism and SERT neurotransmitter maps was localized in the in PCC [MNI XYZ coordinates= 8 -66 42, T=7.45, FWE-corrected p<0.001] (**Figure 4**).

Discussion

A recent clinicopathological study showed that EO-DLB and LO-DLB are largely similar in core symptoms and with a comparable distribution of limbic and neocortical Lewy pathology [5]. However, LO-DLB patients present more amnestic deficits that were accounted for by AD co-pathology, and EO-DLB can be predated by history of depression [5]. The present study shows similarities between EO-DLB and LO-DLB in terms of clinical core symptom presentations and major brain hypometabolism hallmarks.

However, we found that the LO-DLB individuals were characterized by a more severe hypometabolism in the dorsolateral frontal cortex, perisylvian/insular cortex and parahippocampal gyrus. The significant hypometabolism in parahippocampal gyri is in keeping with other structural grey-matter studies [25]. This is consistent also with amyloid and p-Tau pathology reported in the medial temporal cortex of DLB

cases, accounting for hypometabolism in the same region [26]. In a subgroup with available CSF data, we found also significantly higher p-Tau pathology in the LO-DLB that may have a role in the parahippocampal hypometabolism found in this group.

On the other hand, the EO-DLB showed more severe hypometabolism in the precuneus/PCC in the direct comparison with LO-DLB. Of note, subclinical depressive symptoms in ageing are linked with neurodegeneration biomarkers in the precuneus, PCC and fronto-temporal regions [27]. Previous studies reported the presence and intensity of depressive mood specifically characterized the clinicopathological cohort of EO-DLB [5]. While we did not find differences between EO and LO-DLB in neuropsychiatric presentations, depression, and apathy can be observed and linked to the above-reported evidence when a large cohort of subjects would be included. We have to underline that our EO-DLB cases did not begin with a psychiatric- or delirium- onset, thus not representing this specific subtype [28].

Differences in EO-DLB and LO-DLB also emerged with the metabolic connectivity approaches. The whole-brain connectivity analysis revealed a severe disruption for both groups, however with some differences. The loss of connectivity arising from the occipital, inferior temporal and cerebellar nodes characterized both the LO-DLB and EO-DLB. Noteworthy, increases and decreases in connectivity were present and differently expressed by EO-DLB and LO-DLB. Specifically, we observed in EO-DLB a higher amount of increased connectivity than in LO-DLB, in particular between frontal and posterior nodes. Increased connectivity among brain regions has been reported in prodromal DLB, Parkinson's disease, multiple sclerosis, traumatic brain injury, and stroke[29, 30]. While the mechanisms behind hyperconnectivity are still being studied, several valuable hypotheses have been proposed, such as adaptive or maladaptive mechanisms [31, 32]. Notably, this literature also reported a pattern of regionally increased functional connectivity during the early stages of neurodegenerative diseases, followed by a decline in connectivity. This might parallel our findings in EO vs. LO-DLB, the latter characterized by a more severe connectivity decrease.

As far as the RSNs analysis, the LO-DLB group showed a loss of connectivity in the dorsolateral prefrontal part of the ATN. Attentional deficits are listed in the consensus clinical criteria for DLB diagnosis and are useful for differential diagnosis with dementia due to AD[33, 34]. Connectivity alterations in ATN were previously described in other studies conducted in DLB patients both in the prodromal and dementia phases [35]. Here it appears a functional marker of LO-DLB.

EO-DLB instead, showed reduced connectivity in the frontal regions in EXN that are consistent with executive dysfunction and frontal connectivity alterations described in previous studies in DLB on both structural white-matter pathology[36] and functional resting-state connectivity[37]. In addition, the RSNs analysis supports the vulnerability of the DMN in EO-DLB - within both its anterior and posterior parts. We found a loss of connectivity from the PCC node to the anterior part of the DMN and a loss of connectivity within the frontal aDMN. The PCC is a cortical region with high levels of metabolic demand and, together with the adjacent precuneus, represents the main hub of the pDMN[38]. Finally, the EO-DLB group

presented a loss of connectivity within the LIN. Significant connectivity loss involved the limbic structures, in particular from amygdala seed and thalamus (Fig. 3). This finding indicates impaired limbic network connectivity and its possible relevance for the association with neuropsychiatric vulnerability previously reported in EO-DLB. Further studies are necessary for confirmation with large EO-DLB cohorts, here prevented by our limited sample size.

The spatial association analysis based on the metabolic differences in neurotransmission showed significant correlations with AChE, GABAa, SERT, DAT neurotransmitter maps and hypometabolism in both EO and LO DLB groups. Here, we found that the typical hypometabolism pattern was mostly driven by the AChT activity, as suggested by the highest correlation coefficient ($r=-0.368$, $p < 0.001$). A widespread dysfunction of AChE activity was found in DLB [36]. Of note, the spatial coherence of AChE deficit and hypometabolism in DLB was reported in a multimodal neuroimaging study and was related to the degeneration of afferent cholinergic neocortical projections arising from the basal nucleus of Meynert[39]. The spatial association analysis based on metabolic differences in neurotransmission supports the hypothesis of a SERT system derangement as a major monoaminergic etiology differentiating EO-DLB from LO-DLB [5]. Indeed, we found a high correlation between hypometabolism and SERT map in EO-DLB, indicating a matched derangement in metabolism and 5-HTT SERT map. Loss of serotonergic neurons in the rostral raphe nuclei was reported in clinically diagnosed and neuropathologically confirmed DLB[40]. According to the Braak staging, the raphe nucleus is a subcortical region early affected by accumulations of Lewy bodies and neurites, even before the dopaminergic substantia nigra[41].

In conclusion, this brain metabolic study using various analytic approaches and in particular connectivity analyses and neurotransmitter mapping revealed commonalities and differences between EO-DLB and LO-DLB. Specific neurotransmitter systems vulnerabilities and the presence of pure or mixed pathologies may have a role in the brain FDG-PET results.

These results add new biological evidence to the DLB syndromes.

We acknowledge some limitations of the study, mostly due to the retrospective observational design. First, a more comprehensive neuropsychological and neuropsychiatric assessment was not available, to account for between-group differences that emerged in previous studies (e.g., [5]). Further, the diagnosis of DLB was not confirmed at autopsy. However, we adopted standardized clinical diagnostic criteria, which showed high specificity in previous autopsy validations[3]. The role of serotonergic system dysfunction in EO-DLB should be confirmed by direct assessment with PET imaging and specific serotonergic tracers.

Declarations

Ethics approval and consent to participate

The study was approved by San Raffaele Hospital of Milan, Italy (Study Protocol FDG PET Metabolic Patterns version n°2) and University of Geneva Ethic Committees (Study Protocol NO 2022-01520, Geneva, Switzerland) and conducted in compliance with the Declaration of Helsinki for the protection of human participants.

Consent for publication

Not applicable.

Funding

The author(s) received no financial support for the research, authorship, and/or publication of this article.

Availability of data and materials

The datasets used and analyzed during the current study are available from the corresponding author upon reasonable request.

Acknowledgements

The authors thank the individuals participating in the study and their families.

Competing interests

The authors declare that they have no competing interests. VG was supported by the Swiss National Science Foundation (projects 320030_169876, 320030_185028 and IZSEZ0_188355), by the Velux foundation (project 1123), by the Schmidheiny foundation, and by the Aetas foundation. VG received financial support for research and/or speaker fees through her institution from Siemens Healthineers, GE Healthcare, Novo Nordisk.

Authors contribution

SPC, AG, DP contributed to conception and design of the study. SPC, AG contributed to the analysis of data or preparing the figures. DP, LJL contributed to the acquisition of data. SPC, AG, CB, LJL, NN, VG, DP contributed to drafting and revision of the text.

References

1. McMurtray A, Clark DG, Christine D, Mendez MF. Early-onset dementia: frequency and causes compared to late-onset dementia. Dement Geriatr Cogn Disord. 2006;21:59–64.
2. Koedam ELGE, Pijnenburg YAL, Deeg DJH, Baak MME, van der Vlies AE, Scheltens P, et al. Early-onset dementia is associated with higher mortality. Dement Geriatr Cogn Disord. 2008;26:147–52.

3. McKeith IG, Boeve BF, Dickson DW, Halliday G, Taylor J-P, Weintraub D, et al. Diagnosis and management of dementia with Lewy bodies: Fourth consensus report of the DLB Consortium. Neurology. 2017;89:88–100.
4. McKeith IG, Ferman TJ, Thomas AJ, Blanc F, Boeve BF, Fujishiro H, et al. Research criteria for the diagnosis of prodromal dementia with Lewy bodies. Neurology. 2020;94:743–55.
5. Sim J, Li H, Hameed S, Ting SKS. Clinical Manifestations of Early-Onset Dementia With Lewy Bodies Compared With Late-Onset Dementia With Lewy Bodies and Early-Onset Alzheimer Disease. JAMA Neurol. 2022;
6. Schaffert J, LoBue C, White III CL, Wilmoth K, Didehbani N, Lacritz L, et al. Risk factors for earlier dementia onset in autopsy-confirmed Alzheimer's disease, mixed Alzheimer's with Lewy bodies, and pure Lewy body disease. Alzheimer's & Dementia. 2020;16:524–30.
7. Sharp SI, Ballard CG, Ziabreva I, Piggott MA, Perry RH, Perry EK, et al. Cortical serotonin 1A receptor levels are associated with depression in patients with dementia with Lewy bodies and Parkinson's disease dementia. Dement Geriatr Cogn Disord. 2008;26:330–8.
8. Vermeiren Y, van Dam D, Aerts T, Engelborghs S, Martin J-J, de Deyn PP. The monoaminergic footprint of depression and psychosis in dementia with Lewy bodies compared to Alzheimer's disease. Alzheimers Res Ther. 2015;7:1–18.
9. Caminiti SP, Sala A, Iaccarino L, Beretta L, Pilotto A, Gianolli L, et al. Brain glucose metabolism in Lewy body dementia: implications for diagnostic criteria. Alzheimers Res Ther. 2019;11:1–14.
10. Perani D. FDG-PET and amyloid-PET imaging: the diverging paths. Curr Opin Neurol. 2014;27:405–13.
11. Kato T, Inui Y, Nakamura A, Ito K. Brain fluorodeoxyglucose (FDG) PET in dementia. Ageing Res Rev. 2016;30:73–84.
12. Seeley WW, Crawford RK, Zhou J, Miller BL, Greicius MD. Neurodegenerative diseases target large-scale human brain networks. Neuron. 2009;62:42–52.
13. Rossor MN, Fox NC, Mummery CJ, Schott JM, Warren JD. The diagnosis of young-onset dementia. Lancet Neurol. 2010;9:793–806.
14. Perani D, della Rosa PA, Cerami C, Gallivanone F, Fallanca F, Vanoli EG, et al. Validation of an optimized SPM procedure for FDG-PET in dementia diagnosis in a clinical setting. Neuroimage Clin. 2014;6:445–54.
15. Perani D, della Rosa PA, Cerami C, Gallivanone F, Fallanca F, Vanoli EG, et al. Validation of an optimized SPM procedure for FDG-PET in dementia diagnosis in a clinical setting. Neuroimage Clin. 2014;6:445–54.
16. Perani D, Della Rosa PA, Cerami C, Gallivanone F, Fallanca F, Vanoli EG, et al. Validation of an optimized SPM procedure for FDG-PET in dementia diagnosis in a clinical setting. Neuroimage Clin. 2014;6:445–54.
17. Caminiti SP, Alongi P, Majno L, Volontè MA, Cerami C, Gianolli L, et al. Evaluation of an optimized [18F] fluoro-deoxy-glucose positron emission tomography voxel-wise method to early support

differential diagnosis in atypical Parkinsonian disorders. Eur J Neurol. 2017;24:687-e26.

18. Iizuka T, Iizuka R, Kameyama M. Cingulate island sign temporally changes in dementia with Lewy bodies. Sci Rep. 2017;7:1–9.
19. Tzourio-Mazoyer N, Landeau B, Papathanassiou D, Crivello F, Etard O, Delcroix N, et al. Automated anatomical labeling of activations in SPM using a macroscopic anatomical parcellation of the MNI MRI single-subject brain. Neuroimage. 2002;15:273–89.
20. Lee DS, Kang H, Kim H, Park H, Oh JS, Lee JS, et al. Metabolic connectivity by interregional correlation analysis using statistical parametric mapping (SPM) and FDG brain PET; methodological development and patterns of metabolic connectivity in adults. Eur J Nucl Med Mol Imaging. 2008;35:1681–91.
21. Jones DT, Machulda MM, Vemuri P, McDade EM, Zeng G, Senjem ML, et al. Age-related changes in the default mode network are more advanced in Alzheimer disease. Neurology. 2011;77:1524–31.
22. Seeley WW, Menon V, Schatzberg AF, Keller J, Glover GH, Kenna H, et al. Dissociable intrinsic connectivity networks for salience processing and executive control. Journal of Neuroscience. 2007;27:2349–56.
23. Shirer WR, Ryali S, Rykhlevskaia E, Menon V, Greicius MD. Decoding subject-driven cognitive states with whole-brain connectivity patterns. Cerebral cortex. 2012;22:158–65.
24. Dukart J, Holiga S, Rullmann M, Lanzenberger R, Hawkins PCT, Mehta MA, et al. JuSpace: A tool for spatial correlation analyses of magnetic resonance imaging data with nuclear imaging derived neurotransmitter maps. Wiley Online Library; 2021.
25. Elder GJ, Mactier K, Colloby SJ, Watson R, Blamire AM, O'Brien JT, et al. The influence of hippocampal atrophy on the cognitive phenotype of dementia with Lewy bodies. Int J Geriatr Psychiatry. 2017;32:1182–9.
26. Lee Y, Jeon S, Park M, Kang SW, Yoon SH, Baik K, et al. Effects of Alzheimer and Lewy Body Disease Pathologies on Brain Metabolism. Ann Neurol. 2022;
27. Touron E, Moulinet I, Kuhn E, Sherif S, Ourry V, Landeau B, et al. Depressive symptoms in cognitively unimpaired older adults are associated with lower structural and functional integrity in a frontolimbic network. Mol Psychiatry. 2022;1–10.
28. McKeith IG, Ferman TJ, Thomas AJ, Blanc F, Boeve BF, Fujishiro H, et al. Research criteria for the diagnosis of prodromal dementia with Lewy bodies. Neurology. 2020;94:743–55.
29. Hillary FG, Grafman JH. Injured brains and adaptive networks: the benefits and costs of hyperconnectivity. Trends Cogn Sci. 2017;21:385–401.
30. Caminiti SP, Pilotto A, Premi E, Galli A, Ferrari E, Gipponi S, et al. Dopaminergic connectivity reconfiguration in the dementia with Lewy bodies continuum. Parkinsonism Relat Disord [Internet]. 2023;108:105288. Available from: https://www.sciencedirect.com/science/article/pii/S1353802023000111
31. Dubbelink KTEO, Schoonheim MM, Deijen JB, Twisk JWR, Barkhof F, Berendse HW. Functional connectivity and cognitive decline over 3 years in Parkinson disease. Neurology. 2014;83:2046–53.

32. Tewarie P, van Dellen E, Hillebrand A, Stam CJ. The minimum spanning tree: an unbiased method for brain network analysis. Neuroimage. 2015;104:177–88.
33. Calderon J, Perry RJ, Erzinclioglu SW, Berrios GE, Dening Tr, Hodges JR. Perception, attention, and working memory are disproportionately impaired in dementia with Lewy bodies compared with Alzheimer's disease. J Neurol Neurosurg Psychiatry. 2001;70:157–64.
34. McKeith IG, Dickson DW, Lowe J, Emre M, O'brien JT, Feldman H, et al. Diagnosis and management of dementia with Lewy bodies: third report of the DLB Consortium. Neurology. 2005;65:1863–72.
35. Boccalini C, Bortolin E, Carli G, Pilotto A, Galbiati A, Padovani A, et al. Metabolic connectivity of resting-state networks in alpha synucleinopathies, from prodromal to dementia phase. Front Neurosci. 2022;16:930735.
36. Lee JE, Park H-J, Park B, Song SK, Sohn YH, Lee JD, et al. A comparative analysis of cognitive profiles and white-matter alterations using voxel-based diffusion tensor imaging between patients with Parkinson's disease dementia and dementia with Lewy bodies. J Neurol Neurosurg Psychiatry. 2010;81:320–6.
37. Sourty M, Thoraval L, Roquet D, Armspach J-P, Foucher J, Blanc F. Identifying dynamic functional connectivity changes in dementia with lewy bodies based on product hidden markov models. Front Comput Neurosci. 2016;10:60.
38. Leech R, Braga R, Sharp DJ. Echoes of the brain within the posterior cingulate cortex. Journal of Neuroscience. 2012;32:215–22.
39. Klein JC, Eggers C, Kalbe E, Weisenbach S, Hohmann C, Vollmar S, et al. Neurotransmitter changes in dementia with Lewy bodies and Parkinson disease dementia in vivo. Neurology. 2010;74:885–92.
40. Benarroch EE, Schmeichel AM, Sandroni P, Parisi JE, Low PA. Rostral raphe involvement in Lewy body dementia and multiple system atrophy. Acta Neuropathol. 2007;114:213–20.
41. Braak H, del Tredici K, Rüb U, de Vos RAI, Steur ENHJ, Braak E. Staging of brain pathology related to sporadic Parkinson's disease. Neurobiol Aging. 2003;24:197–211.

Figures

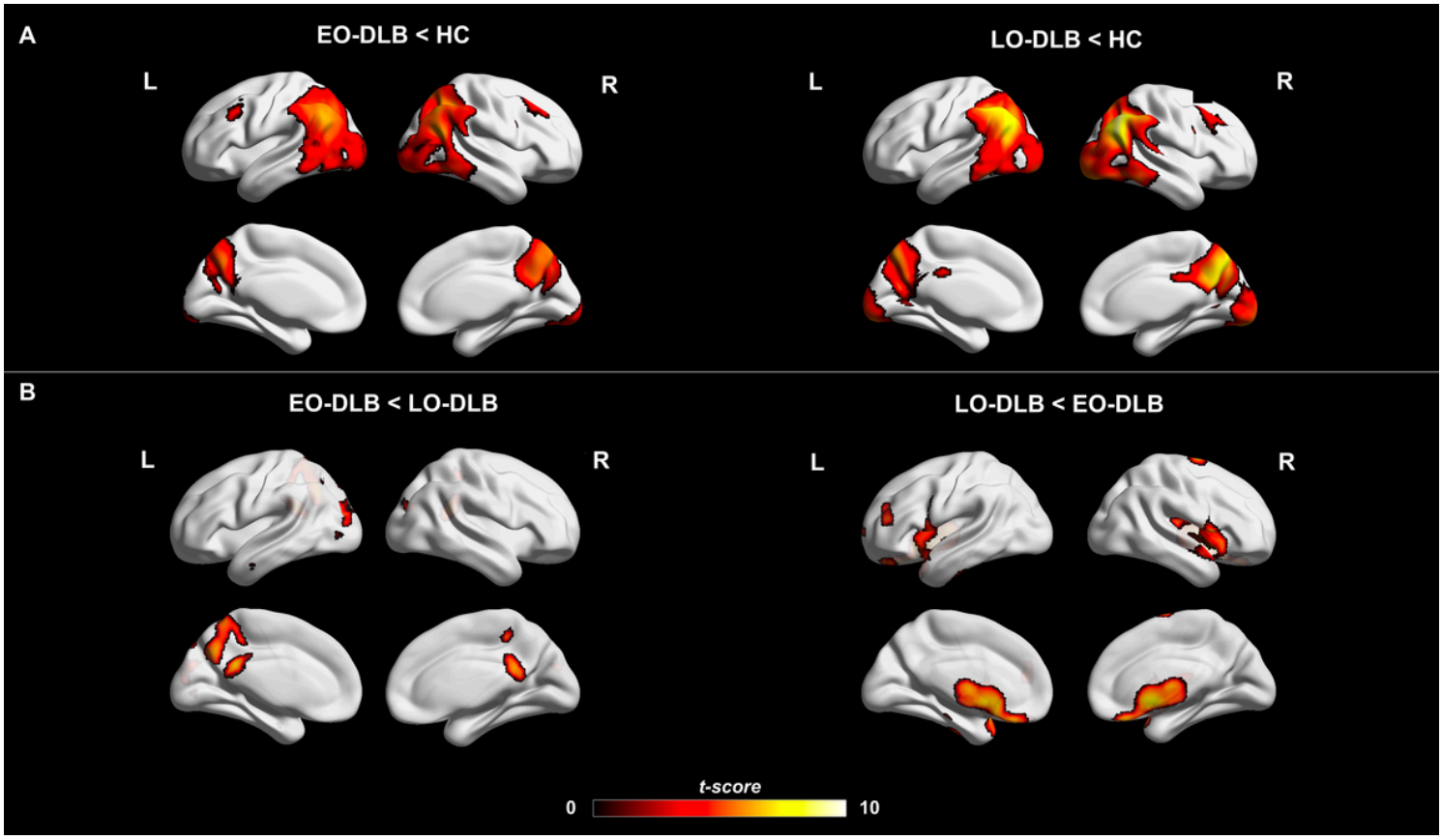

Figure 1

Group-analysis – (A) Voxel-wise SPM comparison between each DLB group and a validated FDG-PET database of HC (N = 112). (B) Voxel-wise SPM direct comparison between EO-DLB (N=21) and LO-DLB (N=41). Hypometabolism is represented in a lateral and medial view. Each comparison was FWE-corrected, with a significance level at $p<0.05$. SPM, Statistical Parametric Mapping; EO-DLB, early-onset dementia with Lewy bodies; LO-DLB, late-onset dementia with Lewy bodies; HC, healthy controls; FWE, Family-wise Error; FDG-PET, Fluorodeoxyglucose-positron emission tomography.

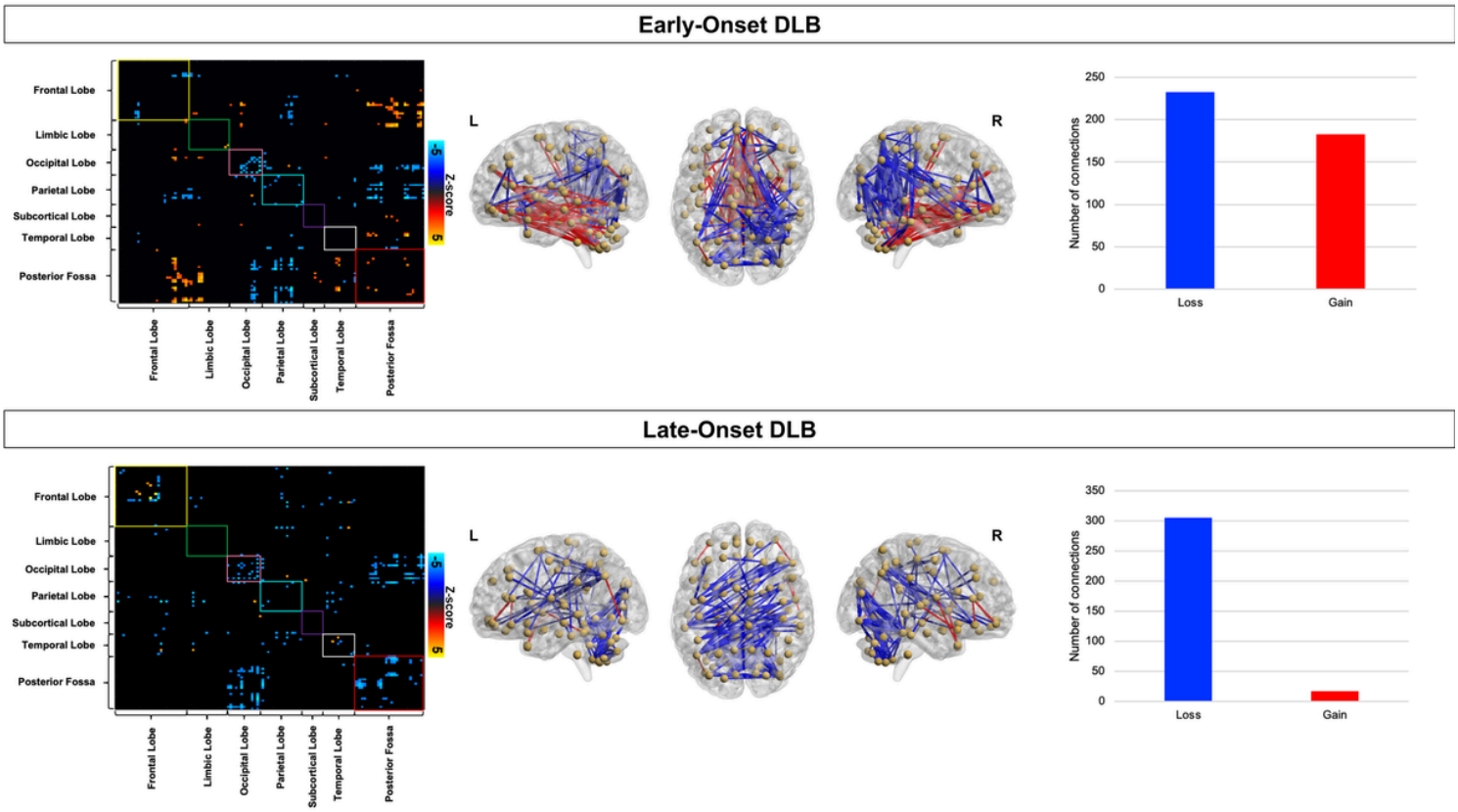

Figure 2

Whole-brain metabolic connectivity architecture – The matrices represent the significant differences obtained comparing adjacency matrices of each clinical cohort (EO-DLB and LO-DLB) with the HC group in the whole-brain network ($p<0.001$). The connectivity loss is shown in cyan-blue, the gained connectivity in yellow-red, and the unchanged connectivity in black. 3D brain showing altered connections (blue edges for losses and red for gains) for EO-DLB and LO-DLB. Box-plot representing number of loss (blue) and gained (red) connections. AAL labels[19] were grouped into 7 macro-ROIs: **Frontal Lobe** (precentral gyrus, superior frontal gyrus, middle frontal gyrus, inferior frontal gyrus, Rolandic operculum, supplementary motor area, olfactory lobe, rectus gyrus), **Limbic Lobe** (insula, anterior cingulate cortex, middle cingulate cortex, posterior cingulate cortex, hippocampus, parahippocampal gyrus, amygdala), **Occipital Lobe** (calcarine cortex, cuneus, lingual gyrus, superior occipital gyrus, middle occipital gyrus, inferior occipital gyrus), **Parietal Lobe** (precentral gyrus, superior parietal lobule, inferior parietal lobule, supramarginal gyrus, angular gyrus, precuneus, paracentral lobule), **Subcortical Lobe** (caudate, putamen, thalamus, pallidum), Temporal Lobe (fusiform gyrus, Heschl gyrus, superior temporal gyrus, superior temporal pole, middle temporal gyrus, middle temporal pole, inferior temporal gyrus), and **Posterior Fossa** (cerebellum crus 1, crus 2, cerebellum 3-10, vermis). EO-DLB, early-onset dementia with Lewy bodies; LO-DLB, late-onset dementia with Lewy bodies; HC, healthy controls; AAL, Automated anatomical labelling atlas.

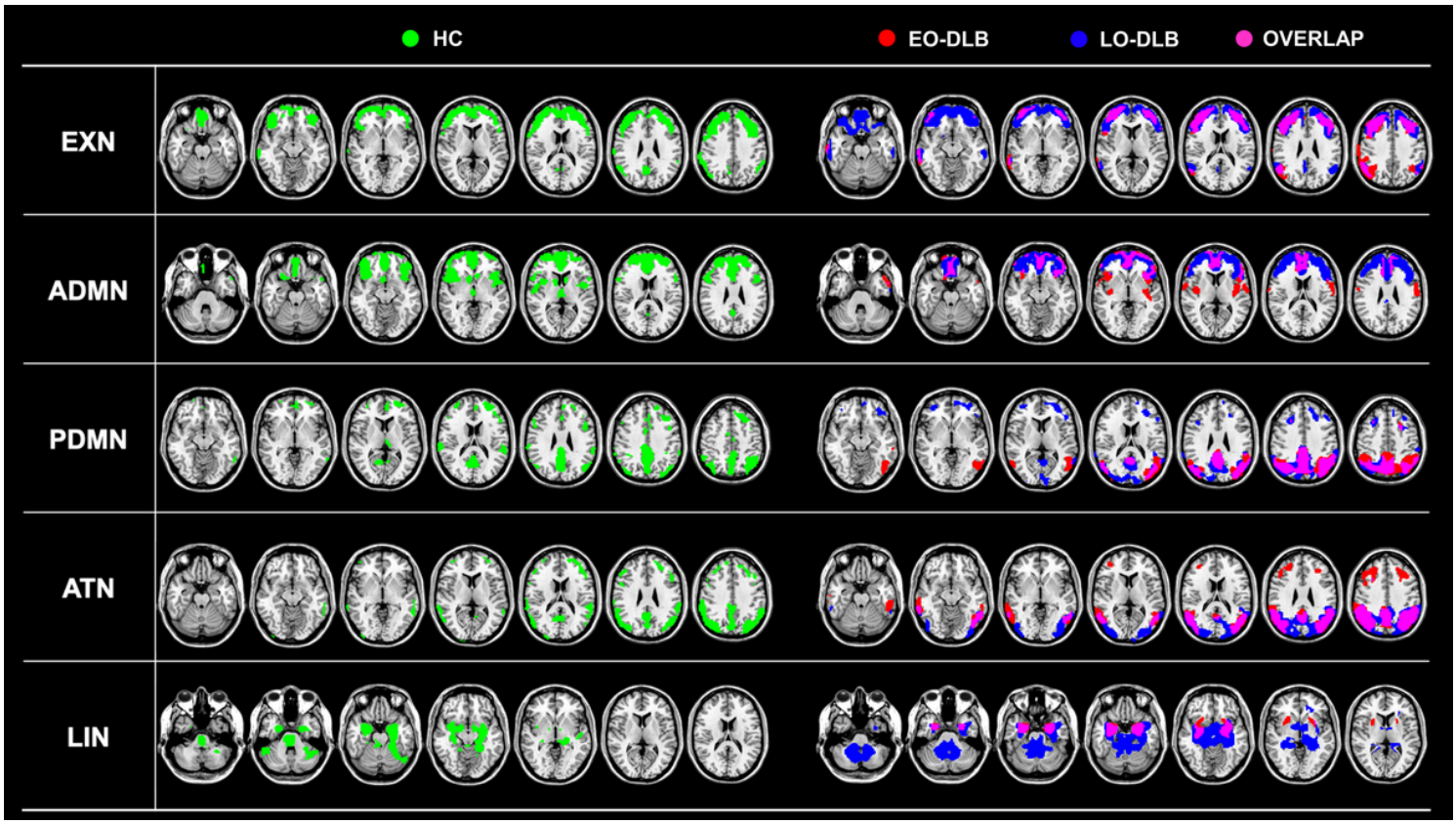

Figure 3

Resting State Networks - Figure illustrates resting-state networks topography in (left) HC (green overlaid to the anatomical template), (right) EO-DLB (red overlaid to the anatomical template) and LO-DLB (blue overlaid to the anatomical template) for anterior and posterior default mode network; attentive, executive networks, limbic network. Overlap in the RSNs between EO-DLB and LO-DLB is represented by pink color. A connectivity derangement is more prominent for EO-DLB than LO-DLB, showing reduced connectivity in the frontal components of the EXN, aDMN and pDMN, and increased connectivity in the LIN. The LO-DLB showed reduced connectivity in ATN. Resting-state networks were obtained using seed-based intercorrelation analysis. Clusters with a minimum spatial extent of 100 voxels are shown, with a voxel-wise significant threshold of $p<0.001$. EO-DLB, early-onset dementia with Lewy bodies; LO-DLB, late-onset dementia with Lewy bodies; HC, healthy controls; aDMN, anterior default mode network; pDMN, posterior default mode network; ATN, attentive network; EXN, executive network, LIN, limbic network.

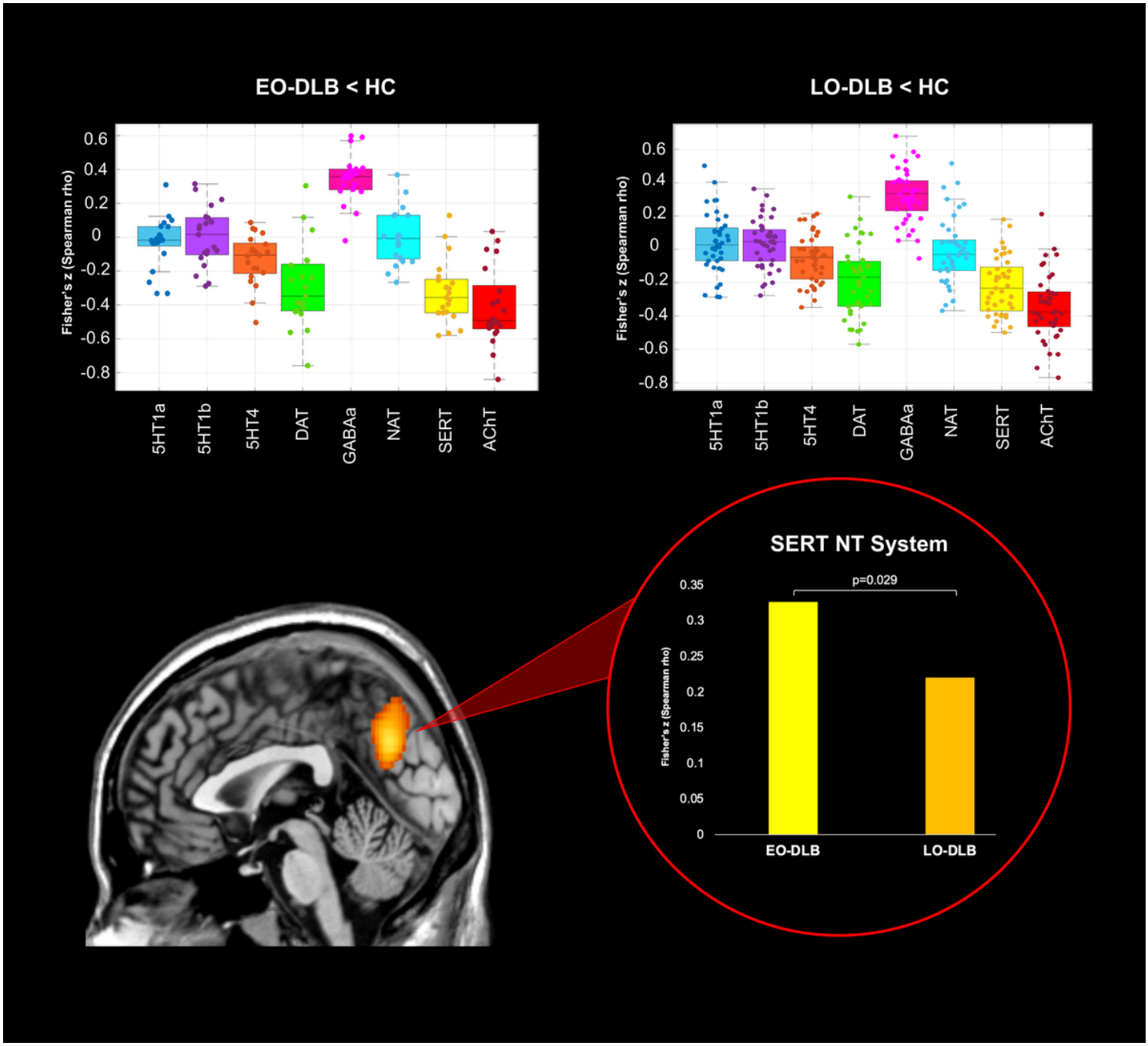

Figure 4

Neurotransmitter topography analysis – (top) Bar plots representing Fisher's z-scores resulting from the Spearman correlation analysis between hypometabolism z-scores and neurotransmitter systems in EO-DLB (left) and LO-DLB (right); (bottom) Bar plot representing the significant difference between the two DLB groups within the serotonin transporter (SERT) circuit resulting from the post-hoc direct comparison (absolute values of Rho Fisher's z). FDG-PET hypometabolism in posterior cingulate cortex overlaid on a T1-template image, which is associated to alterations within the serotonergic network. Significance level was set at FWE-p<0.05. EO-DLB, early-onset dementia with Lewy bodies; LO-DLB, late-onset dementia with Lewy bodies; HC, healthy controls; FDG-PET, Fluorodeoxyglucose-positron emission tomography.